



Article

# Date Palm Leaflet-Derived Carbon Microspheres Activated Using Phosphoric Acid for Efficient Lead (II) Adsorption

Saeed Alhawtali <sup>1</sup>, Mohanad El-Harbawi <sup>2,\*</sup>, Lahssen El Blidi <sup>1</sup>, Maher M. Alrashed <sup>1</sup>, Abdulrahman Alzobidi <sup>1</sup> and Chun-Yang Yin <sup>2</sup>

<sup>1</sup> Department of Chemical Engineering, King Saud University, Riyadh 11421, Saudi Arabia; saeerr2014@gmail.com (S.A.); lelblidi@ksu.edu.sa (L.E.B.); mabdulaziz@ksu.edu.sa (M.M.A.); abduh1414@gmail.com (A.A.)

<sup>2</sup> SIT Building @ Ngee Ann Polytechnic, Newcastle University in Singapore, 537 Clementi Road #06-01, Singapore 599493, Singapore; chunyang.yin@newcastle.ac.uk

\* Correspondence: melharbawi@ksu.edu.sa

**Abstract:** The removal of lead metals from wastewater was carried out with carbon microspheres (CMs) prepared from date palm leaflets using a hydrothermal carbonization process (HTC). The prepared CMs were subsequently activated with phosphoric acid using the incipient wetness impregnation method. The prepared sample had a low Brunauer–Emmet–Teller (BET) surface area of  $2.21 \text{ m}^2 \cdot \text{g}^{-1}$ , which increased substantially to  $808 \text{ m}^2 \cdot \text{g}^{-1}$  after the activation process. Various characterization techniques, such as scanning electron microscopy, BET analysis, Fourier transform infrared, and elemental analysis (CHNS), were used to evaluate the morphological structure and physico-chemical properties of the CMs before and after activation. The increase in surface area is an indicator of the activation process, which enhances the absorption properties of the material. The results demonstrated that the activated CMs had a notable adsorption capacity, with a maximum adsorption capacity of  $136 \text{ mg} \cdot \text{g}^{-1}$  for lead (II) ions. This finding suggests that the activated CMs are highly effective in removing lead pollutants from water. This research underscores the promise of utilizing activated carbon materials extracted from palm leaflets as an eco-friendly method with high potential for water purification, specifically in eliminating heavy metal pollutants, particularly lead (II), contributing to sustainability through biomass reuse.

**Keywords:** date palm leaflet; hydrothermal carbonization; carbon microspheres; activation; lead; adsorption



**Citation:** Alhawtali, S.; El-Harbawi, M.; El Blidi, L.; Alrashed, M.M.; Alzobidi, A.; Yin, C.-Y. Date Palm Leaflet-Derived Carbon Microspheres Activated Using Phosphoric Acid for Efficient Lead (II) Adsorption. *C* **2024**, *10*, 26. <https://doi.org/10.3390/c10010026>

Academic Editors: Jinliang Song and Jorge Bedia

Received: 5 January 2024

Revised: 11 February 2024

Accepted: 20 February 2024

Published: 12 March 2024



**Copyright:** © 2024 by the authors. Licensee MDPI, Basel, Switzerland. This article is an open access article distributed under the terms and conditions of the Creative Commons Attribution (CC BY) license (<https://creativecommons.org/licenses/by/4.0/>).

## 1. Introduction

The rapid growth of industry and industrial activities has resulted in a significant increase in the volume of industrial wastewater. This wastewater often contains various pollutants and contaminants that can pose significant environmental and health risks if not properly managed. The presence of dyes and toxic heavy metals in industrial effluents is a significant concern, given their potential to cause environmental and human health risks. Governments and regulatory agencies around the world have recognized the need to control and mitigate the discharge of such pollutants into water bodies [1,2]. Dyes and heavy metals can be effectively removed from wastewater through various treatment methods such as adsorption, membrane filtration, ion exchange, coagulation, electrochemistry, electrochemical removal, and chemical precipitation [3,4]. Although numerous techniques for treating wastewater can effectively eliminate dyes and heavy metals, several of these methods pose substantial limitations and difficulties. These include considerable initial investment, high energy demands, incomplete pollutant removal, high upkeep and operational expenses, lengthy regeneration processes, and the generation of hazardous sludge [5,6]. Adsorption is widely regarded as one of the most efficient and cheapest methods for removing various aqueous pollutants from wastewater. This

method offers several advantages, making it a popular choice in the domain of wastewater treatment [7]. Carbon materials have become essential for adsorption applications because of their significant surface area, extensive pore volume, and diverse pore structure [8,9]. Carbon materials can be produced from different natural precursors, such as agricultural wastes. Various studies have sought to transform agricultural waste into low-cost carbon materials due to the abundance of agricultural waste in various parts of the world. Date palms are among the most widespread trees in Arab countries. Palm trees produce large amounts of biomass such as fronds, empty fruit bunch, and fibers. One tree produces the equivalent of 20 kg of waste per year, which is a huge burden in disposing of these large quantities. Such agricultural activities generate large amounts of biomass waste that not only cause disposal problems, but also waste a potentially valuable resource. Agricultural biomass waste is usually disposed of by incineration using conventional methods, releasing unhindered hazardous flue gasses such as soot, NO<sub>x</sub>, SO<sub>x</sub>, etc. It is noteworthy that products made from bamboo or coconut shells have seen widespread commercial utilization. In contrast, there is untapped potential for effectively utilizing date palm waste, and the industry has yet to fully explore commercial applications for this resource. Palm tree waste contains a high proportion of cellulose, and can therefore be recycled and converted into carbonaceous materials such as hydrochar, with a high absorption capacity. Hydrochar is a high-carbon material that can be produced by a hydrothermal carbonization (HTC) process. In comparison to other processes such as pyrolysis, carbonization, and activation, this process is thought to be economical and environmentally beneficial because it is carried out at a low temperature (180 to 250 °C). The hydrochar produced by this process, however, has poor physical properties, including a low surface area, low porosity, and deficiency of weakly acidic functional groups [10]. These properties can limit its effectiveness for various applications. Chemical activation using various chemicals, such as phosphoric acid, potassium hydroxide, nitric acid, acrylic acid, and citric acid is a common method used to enhance the physico-chemical properties of hydrochar, making it more suitable for specific purposes. Diaz and coresearchers used KOH, FeCl<sub>3</sub>, and H<sub>3</sub>PO<sub>4</sub> to activate hydrochar prepared from grape seeds [11] and olive stones [12]. The results showed that KOH was the activating agent that allowed the highest BET surface area values of up to 2200 m<sup>2</sup>·g<sup>-1</sup>. The material activated with KOH gave a removal capacity of 650 mg·g<sup>-1</sup> for sulfamethoxazole. Adebisi et al. [13] used H<sub>3</sub>PO<sub>4</sub> to activate hydrochar-made empty banana fruit bunch fibers. The BET surface area was increased from 7.01 to 762.05 m<sup>2</sup>·g<sup>-1</sup> after activation. The prepared material was able to remove Pb (II) and Zn (II) with removal capacities of 74.6 and 77.5 mg·g<sup>-1</sup>, respectively. Shi et al. [14] obtained a high BET surface area, 3580 m<sup>2</sup>·g<sup>-1</sup>, using KHCO<sub>3</sub> to treat hydrochar derived from glucose. The material exhibited excellent CO<sub>2</sub> capture capabilities of 35.6 mmol·g<sup>-1</sup>. Congsomjit and Areeprasert [15] used steam to activate hydrochar prepared from sugar cane bagasse and used it for syrup decolorization. Hayoun et al. [10] synthesized hydrochar from loquat cores via hydrothermal carbonization assisted with citric acid and used the product for the removal of prednisolone, diclofenac, and antipyrine. Koprivica and coworkers [16] prepared alkali-modified hydrochar from *Paulownia* leaves and employed it to remove Pb (II). Zhang et al. [17] synthesized a potassium permanganate-modified hydrochar and used it for the sorption of Pb (II), Cu (II), and Cd (II).

Lead, a prevalent heavy metal, presents substantial risks to both the environment and human health. In nature, lead exists either as lead sulfide or in an ore complex with zinc sulfide [18,19]. Several industrial operations, including mining, battery production, chemical manufacturing, petroleum refining, plastic manufacturing, and the building industry, discharge lead and its byproducts into aquatic ecosystems [19–21]. The extraction of lead ions from both potable water sources and wastewater is essential to safeguard the environment and guarantee a secure and pristine water supply. The removal of lead ions has been reported in several publications. In recent years, hydrochar made from various biomass sources has been used as an adsorbent to remove lead ions from water and wastewater. For instance, Nzediegwu et al. [22] synthesized hydrochar from canola

straw and found that it had a maximal absorption capacity of  $24.4 \text{ mg}\cdot\text{g}^{-1}$ . The hydrochar produced by Rasam et al. [23] from *Crocus sativus* petals activated with zinc chloride had a maximum absorption capacity of  $89.5 \text{ mg}\cdot\text{g}^{-1}$ . Petrović et al. [24] utilized grape pomace to prepare hydrochar, which was subsequently activated with potassium hydroxide. A maximum absorption capacity of  $137 \text{ mg}\cdot\text{g}^{-1}$  was achieved. Zhou et al. [25] and Ge et al. [26] utilized fresh banana peels and prepared phosphoric acid-activated hydrochar with maximum absorption capacities of 241 and  $238 \text{ mg}\cdot\text{g}^{-1}$ , respectively.

In the present study, cellulose materials (CMs) were synthesized using date palm (*Phoenix dactylifera*) leaflets as the precursor, followed by activation with phosphoric acid to optimize sorption characteristics and enhance lead removal efficiency. The distinct focus on lead removal, particularly utilizing CMs derived from date palm leaflets, represents a novel and unexplored opportunity within the scientific literature. This research addresses a significant gap in our current understanding, as no prior investigations have systematically examined the potential of phosphoric acid-activated CMs derived from date palm leaflets for lead removal. The outcomes of this study are envisioned to contribute invaluable insights to the scientific community, advancing our understanding of strategies for alleviating lead contamination in environmental and industrial settings.

## 2. Experimental

### 2.1. Raw Materials and Reagents

Palm leaves were gathered from a farm in Riyadh, Saudi Arabia. The collected palm leaves were initially cleaned using laboratory compressed air. This step was intended to remove loose dust and particles that may have settled on the surface of the leaves during collection and transportation. Subsequently, the leaves were washed numerous times with both tap and distilled water to remove dusts adhering to the surface. Then, the biomass was dried at  $80 \text{ }^\circ\text{C}$  in a laboratory dryer for two days. The leaflets were then processed via a Pulverisette 15 cutting mill (Fritsch, GmbH, Hamburg, Germany) into a fine powder. The powder was then manually sieved via a standard sieve size 60 mesh. As described in the authors' previous studies, a size of  $250 \text{ }\mu\text{m}$  was chosen for the HTC process [27–29].

Ethanol (96%) was purchased from PanReac AppliChem ITW Reagents, Castellar del Valees, Spain, and was used only to remove the synthesized solid materials produced by the HTC process. Phosphoric acid (85 wt% in  $\text{H}_2\text{O}$ , Sigma-Aldrich, St. Louis, MO, USA) was used to activate the CMs prepared by the HTC process. Lead (II) sulfate (98%) was also purchased from Sigma-Aldrich Company Ltd., St. Louis, MO, USA. Milli-Q (Direct Q-5, Merck Millipore, Billerica, MA, USA) ultrapure water ( $18.2 \text{ M}\Omega \text{ cm}$ ) was used for HTC, washing of the HTC products, preparation of the lead solution, and adsorption processes.

### 2.2. Preparation of Carbon Microspheres

A total of 2.5 g of leaflets, possessing a particle diameter of  $250 \text{ }\mu\text{m}$ , was placed into conical flasks containing 25 mL of deionized water. Subsequently, the mixture underwent agitation with a magnetic stirrer for approximately 5 h. The obtained samples were then transferred to Teflon-lined PARR reactors with a volume of 45 mL for the hydrothermal carbonization (HTC) process. As described in our previous work [27], the PARR reactors were subjected to 8 h of heating at  $230 \text{ }^\circ\text{C}$  within a muffle furnace, securely sealed during the entire heating period. After the completion of the HTC process, the PARR vessels were removed from the muffle furnace and allowed to cool down to room temperature. The resulting dark, viscous liquid, containing residual solids, underwent multiple rinses with deionized water and ethanol. The mixture was then drained through a vacuum filtration system to separate the solid particles. The wet solid product obtained from filtration was dried in a drying oven at  $80 \text{ }^\circ\text{C}$  for 24 h. The resulting dry solid was subsequently pulverized using a mortar and pestle, and stored in airtight containers within a desiccator before undergoing the activation process.

### 2.3. Activation of the CMs

Although the HTC process is an efficient, economical, and environmentally friendly process for converting biomass into valuable carbon materials, these materials generally suffer from a low surface area, resulting in a low adsorption capacity. High-specific surface areas are often produced by chemical activation. Therefore, the prepared sample was activated with phosphoric acid using the incipient wetness impregnation method [29–31]. The effects of activation temperature and phosphoric acid concentrations were taken from the authors' earlier investigation [29]. Briefly, a dropwise solution of 3.5 mL (85%) phosphoric acid was added to a 1 g CM sample prepared according to the HTC process, followed by vigorous and constant agitation of the sample, resulting in the formation of a thin phosphoric acid film on the sample's surface. The impregnated sample was subsequently dried overnight at 80 °C and calcined according to the following program, from 20 °C to 550 °C at 10 °C·min<sup>-1</sup> and 550 °C for 90 min under N<sub>2</sub> flow in a horizontal tube furnace (OTF-1200X-S, MTI, Richmond, VA, USA). The resultant products were repeatedly rinsed with deionized water until the desired neutral pH was achieved, filtered, then dried at 80 °C for a period of 24 h. Samples are designated as "UAL" (unactivated leaflets), "L-Cal" (calcined leaflets), "AL" (activated leaflets), and "ALAA" (activated leaflets after adsorption). Finally, the prepared materials were stored in a desiccator before being used for lead removal.

### 2.4. Characterization of CMs and Activated CMs

The prepared materials were characterized prior and after activation using a Tuscan scanning electron microscope (SEM), VEGA II LSU (Tuscan USA Inc., Tucson, AZ, USA). The diameter of CMs was calculated using the ImageJ software (version 1.53t, National Institute of Health (NIH), USA, Bethesda, MD, USA). Brunauer–Emmett–Teller (BET) surface area, pore diameter, and pore volume were determined using a Micromeritics ASAP 2020 (Norcross, GA, USA) surface analyzer, with the BJH (Barrett–Joyner–Halenda) method employed for both the determination of pore volume and pore size. The CM samples were degassed at 200 °C under vacuum for 3 h, and their surface area was calculated using nitrogen adsorption–desorption isotherms. The samples were subjected to an elemental analysis using a PerkinElmer series II CHNS/O 2400 analyzer (VELP, Boston, MA, USA). Through calculating the remaining mass, the oxygen content was determined. To ascertain the existence of particular surface functional groups, both prior and following activation samples were analyzed by a Fourier transform infrared (FTIR) spectroscopy system Shimadzu IRPrestige-21 (Shimadzu, Tokyo, Japan). The analysis conditions employed were 16 scans in the 4000 to 500 cm<sup>-1</sup> wavenumber range and with a spectral resolution wavenumber of 4 cm<sup>-1</sup>. The pellet samples were mixed with KBr prior to analysis.

### 2.5. Adsorption Studies

The adsorption experiment was performed in batch mode to evaluate the adsorptive capability of the obtained activated CMs for the removal of lead (II). To investigate the influence of various parameters on the process of adsorption, such as pH, contact time, quantity of adsorbent, and heavy metal initial concentration, batch adsorption experiments were conducted several times as a series.

Lead (II) was dissolved as lead nitrate in deionized water to obtain a desired concentration of 2000 mg·L<sup>-1</sup> of the stock solution. To adjust the pH of the lead solution to 6, sodium hydroxide (0.1 M) and hydrochloric acid (0.1 M) were used. A hydrogen ion concentration meter was used for the measurement of the pH of heavy metal solutions. Volumes of 250 mL of lead solution with initial concentrations between 50 and 500 mg·L<sup>-1</sup> were added to 350 mL Erlenmeyer flasks and measured accurately. To achieve the adsorption equilibrium at 25 °C, 0.125 g of the activated samples were added to each flask and agitated for 300 min at a speed of 150 rpm in a shaker. During the batch adsorption experiment, 10 mL of supernatant was extracted from each flask at predetermined time intervals. After

that, the supernatant was centrifuged for 6 min at a speed of 5000 rpm using a centrifuge, Hettich (EBA 20), to separate any suspended particles. A tiny amount (2 mL) of supernatant was taken out of the centrifuged bottle and mixed with deionized water and then stored in sealed bottles for atomic absorption spectrophotometry (Shimadzu AA-7000) analysis. The remaining 8 mL was then put back into the flask to prevent the adsorbent from being lost. Through comparing the absorbance with the calibration curve, the concentration of lead (II) was determined. Adsorbed total lead (II),  $q_t$  ( $\text{mg}\cdot\text{g}^{-1}$ ), at a time  $t$  on CMs was determined using Equation (1),

$$q_t = \frac{(C_o - C_t) V}{M} \quad (1)$$

where  $q_t$  ( $\text{mg}\cdot\text{g}^{-1}$ ) denotes the adsorption amount at time  $t$ ,  $C_o$  is the initial solution concentration ( $\text{mg}\cdot\text{L}^{-1}$ ),  $C_t$  is the solution concentration at time  $t$  ( $\text{mg}\cdot\text{L}^{-1}$ ),  $V$  is the solution volume (L), and  $M$  is the mass of the heavy metal adsorbent (g).

To determine the adsorption rate of lead (II) at equilibrium,  $q_e$  ( $\text{mg}\cdot\text{g}^{-1}$ ), Equation (2) can be employed,

$$q_e = \frac{(C_o - C_e) V}{M} \quad (2)$$

where  $q_e$  ( $\text{mg}\cdot\text{g}^{-1}$ ) denotes the adsorption amount at equilibrium, and  $C_e$  represents the equilibrium solution concentration ( $\text{mg}\cdot\text{L}^{-1}$ ).

In contrast, the removal efficiency can be established via Equation (3):

$$R(\%) = \frac{(C_o - C_e)}{C_o} \times 100 \quad (3)$$

The pH<sub>pzc</sub> value of the activated sample was determined using a procedure customized from reported studies [32,33]. Initially, multiple closed Erlenmeyer flasks were filled with 50 mL of a NaCl 0.01 M solution. Each flask's pH was adjusted to a value between 2 and 10 by adding solutions of either 0.1 M NaOH or 0.1 M HCl. Each flask was then filled with an amount of 0.15 of the sample and, after 48 h of agitation at room temperature, the final pH was determined. The point at which the pH final vs. pH initial curve crosses the pH final = pH initial line defines the pH<sub>pzc</sub>. For each of the activated samples, the procedure was repeated. To completely remove the impact of CO<sub>2</sub> on pH, N<sub>2</sub> was flashed onto the solutions for 10 min.

### 2.6. Multistage Remove and Unregenerated Reuse of Adsorbent

In order to achieve deep adsorption of lead (II), a sequence of adsorption cycles was performed. In this way, after a first extraction cycle, the treated lead (II) solution was filtered and exposed to fresh AL. This process was repeated until an extremely low concentration of lead (II) was obtained.

Additionally, a study on unregenerated reuse was conducted to evaluate the ability of the adsorbent to reabsorb lead (II) ions and inspect its adsorption capacity without undergoing a regeneration or washing step between uses. The activated sample underwent a reusability study with multistage adsorption, where 200 mL of a lead-containing solution was introduced to 100 mg of the AL. The experiment was conducted at room temperature for 300 min. After adsorption, the adsorbent must be effectively separated from the solution to isolate all suspended particles by filtration. The reusability of the adsorbent was assessed by reintroducing the unregenerated adsorbent to a new 200 mg/L of lead (II) solution for an additional 300 min. This process was repeated for three adsorption stages, each aiming to test the adsorbent's performance. To gauge the effectiveness of the adsorbent in each stage of the batch adsorption process, the percentage of removal (%) was calculated.

## 3. Results and Discussions

Table 1 shows the BET surface areas for the three samples: before activation, UAL, calcined without H<sub>3</sub>PO<sub>4</sub>, L-Cal, and after activation, AL. The UAL sample exhibited a low

surface area of about  $2.2 \text{ m}^2 \cdot \text{g}^{-1}$ , indicating very low porosity. It had a biomass conversion yield of 52%. In contrast to the UAL sample, L-Cal showed an increase in surface area, reaching  $268.71 \text{ m}^2 \cdot \text{g}^{-1}$ . AL, on the other hand, showed a significant increase in surface area of  $808 \text{ m}^2 \cdot \text{g}^{-1}$  after treatment with phosphoric acid, as pores formed on the microspheres' surfaces. This shows that the internal pores were not fully formed on the CM particles prior to activation. As shown in Table 1, the pore volume of L-Cal and AL increased dramatically after activation. From the data presented in Table 1, the three samples can be classified as mesoporous, in line with the International Union of Pure and Applied Chemistry (IUPAC) categorization, with pore sizes ranging from 3.33 nm to 18.04 nm.

**Table 1.** The CMs' BET surface area, pore volume, and pore size.

Sample	BET Surface Area ( $\text{m}^2 \cdot \text{g}^{-1}$ )	Pore Volume ( $\text{mL} \cdot \text{g}^{-1}$ )	Pore Size (nm)
UAL	2.21	0.0086	18.04
L-Cal	268.71	0.119	8.46
AL	808	0.156	3.33

Figure S1 shows the pore size distribution of the synthesized samples and nitrogen physisorption isotherms. The  $\text{N}_2$  adsorption in UAL's isotherms only became noticeable at low relative pressure, which indicates the isotherms belong to type I in the IUPAC classification. UAL exhibited microporosity with a small fluctuation in uptake seen at slightly higher  $P/P^\circ$  values. L-Cal and AL, on the other hand, is classified as quasi-type IV due to the small hysteresis loops, indicating minor mesoporosity, but it cannot be purely classified as type IV because of the absence of a plateau at the end of hysteresis. L-Cal and AL have increased pore volumes due to the presence of mesoporosity within the 20 to 50 Ångstrom range. The Barrett–Joyner–Halenda (BJH) method was used for both the determination of pore volume and pore size. The mesopores may exhibit selective adsorption behavior. Different pores sizes can preferentially adsorb certain ions based on their size and chemical properties. In the case of lead (II), the mesopores in this range might offer optimal conditions for effective adsorption, i.e., improvement of the diffusion of lead (II) ions into the interior of the carbon microspheres, thereby promoting faster adsorption kinetics. On the other hand, smaller pores may lead to slower kinetics due to restricted diffusion, while larger pores might allow for quicker access, but may not provide sufficient adsorption sites.

The spherical aggregates that are typical of HTC biomass are presented in Figure 1, which examines the morphology of three samples: UAL (before activation), L-Cal (calcined without  $\text{H}_3\text{PO}_4$ ), and AL (after activation) using SEM. Figure 1a illustrates microspheres' tendency to aggregate, forming spherical nuclei with an average diameter of approximately  $6 \mu\text{m}$ . Meanwhile, Figure 1b displays the morphology of CMs at  $230^\circ\text{C}$  and 8 h after calcination without  $\text{H}_3\text{PO}_4$  treatment, where microspheres continue to exhibit a propensity to aggregate. Finally, Figure 1c depicts the microspheres' morphology at  $230^\circ\text{C}$  and 8 h following activation, showing their tendency to aggregate and form spherical nuclei with an average diameter of about  $6 \mu\text{m}$ , despite activation. It is noteworthy that while the CMs maintain their average size and propensity to aggregate after activation, the overall morphology is not as uniform as observed in simple sugars such as glucose [34].

The elemental analysis (C, H, O, N, and S) for the raw leaflets, UAL, and AL results are summarized in Table 2. The elemental contents of C, H, O, N, and S in the AL sample were 70.1, 2.57, 1.24, 25.4, and 0.72 wt%, respectively. Clearly, the AL sample gave the highest percentage of C, 70.1%, followed by the UAL sample, 59.0%. The alterations in elemental profile from biomass to HTC carbon microspheres were thoroughly examined using the traditional van Krevelen diagram, as shown in Figure 2. Based on the diagram, the shifts seen in the two atomic ratios (O/C and H/C) from biomass to microspheres (hydrochars) align with a dehydration process [27].

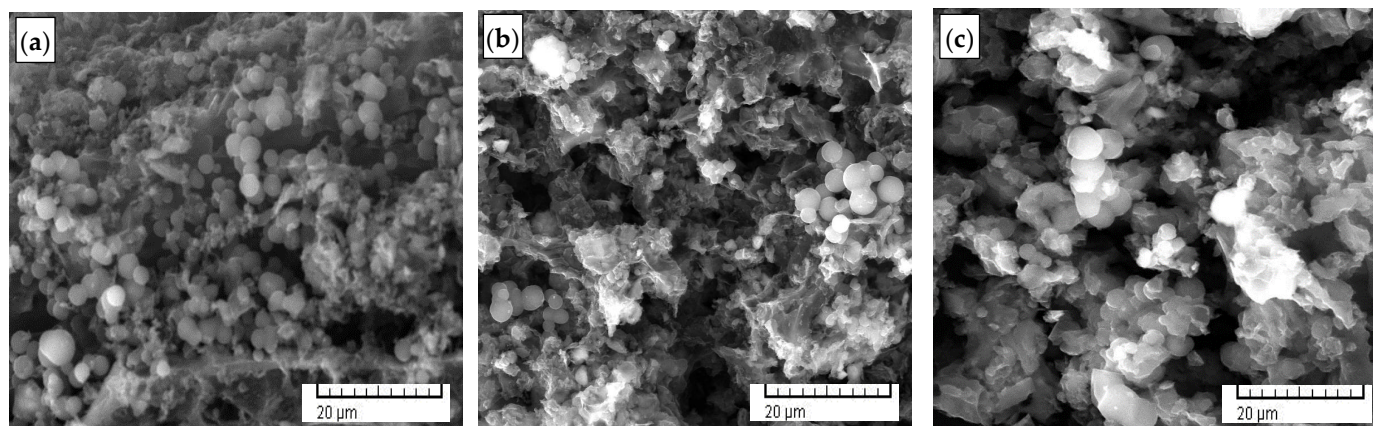


**Figure 1.** SEM images of the synthesized CMs (a) UAL sample, (b) L-Cal sample, and (c) AL sample.

**Table 2.** Elemental analysis for raw leaflets, UAL, and AL Samples.

Sample	Chemical Composition					O/C (Atomic)	H/C (Atomic)
	C (wt%)	H (wt%)	N (wt%)	S (wt%)	O (wt%)		
Raw *	46.50	5.69	0.66	-	47.15	0.90	1.50
UAL	58.99 ± 0.53	6.58 ± 0.13	21.65 ± 0.24	0.92 ± 0.007	11.86 ± 0.13	0.15	1.34
AL	70.12 ± 0.63	2.57 ± 0.05	25.35 ± 0.27	0.72 ± 0.006	1.24 ± 0.01	0.01	0.44
L-Cal	65.36 ± 0.74	3.74 ± 0.09	24.52 ± 0.31	0.78 ± 0.006	5.60 ± 0.08	0.06	0.69

\* Raw leaflets [35].

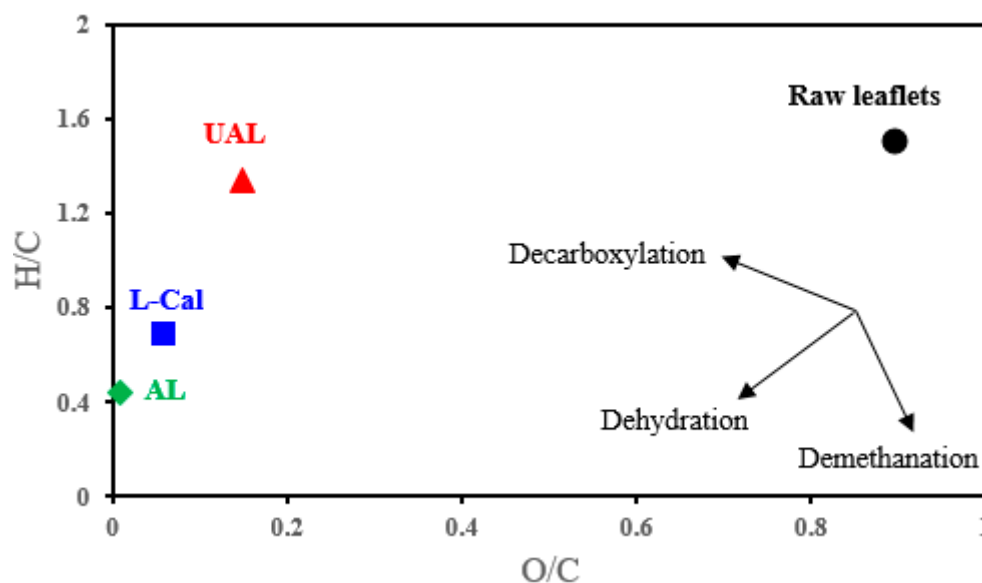


**Figure 2.** The van Krevelen diagram for raw leaflets, unactivated leaflets (UAL), and activated leaflets (AL).

The UAL, L-Cal, and AL materials were analyzed using FTIR (Figure 3). The samples' main peaks were visible at approximately 1090, 1519, 1565, 1630, 2900, and 3350 to 3450  $\text{cm}^{-1}$  [29,36,37]. All samples presented the characteristic peak of the widening vibration of the C=O carbonyl group at 1665  $\text{cm}^{-1}$ , while the peak at 2900  $\text{cm}^{-1}$  represents the presence of aliphatic C-H groups. The bands at 1519  $\text{cm}^{-1}$  are assigned to C=C. The -OH rounded broad band appeared at 3350 to 3450  $\text{cm}^{-1}$ . The vibration band 1080  $\text{cm}^{-1}$  is due to the broadening of the C-O group [29]. A potential vibration might be related to P=O stretching in phosphate (or polyphosphate) groups at around 1300  $\text{cm}^{-1}$ . The presence of

these functional groups is consistent with regularly produced hydrochars originating from agricultural biomass, according to the FTIR data [38,39].

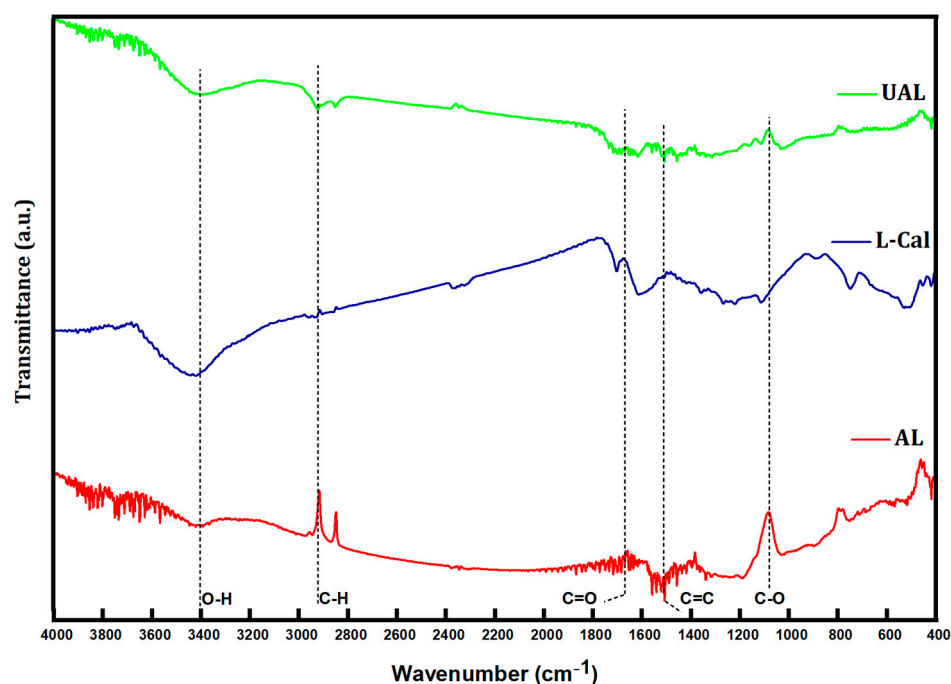


**Figure 3.** FTIR spectra for the UAL, L-Cal, and AL samples.

### 3.1. Adsorption Studies

#### 3.1.1. Effect of pH

The adsorption properties of a material can be affected by a change in pH, which is caused by the protonation/deprotonation of the adsorbed material [40]. The influence of initial pH on the removal of lead (II) onto the prepared CMs was examined at different pH values, ranging from pH 2 to 7. The fixed constant parameter concentration of  $200 \text{ g}\cdot\text{L}^{-1}$  of heavy metal ions and an adsorbent dose of  $0.25 \text{ g}\cdot\text{L}^{-1}$  was used in this study. The pH<sub>pzc</sub> relates to the zero surface charge density, that is, to equal amounts of negative and positive charges generated by proton equilibria [41]. Therefore, the establishment of the pH<sub>pzc</sub> would essentially give an inclination of the specificity of adsorption. The pH<sub>pzc</sub> of the sample was determined to be 2.39 (Figure S1 in the Supplementary Materials), which can be compared to the pH<sub>pzc</sub> of palm shell activated carbon (1.43) reported by Issabayeva and coresearchers [41]. Mullet and coresearchers [42] indicated that greater adsorption of metal ions on the surface was stimulated when the solution pH was greater than pH<sub>pzc</sub>. Since the pH<sub>pzc</sub> was found to be relatively low, lead ion adsorption could be expected to be facilitated within the pH range from 2.5 to 6.

Results showed that at a pH level of 2, the AL particles were positively charged, causing them to repel lead (II) ions from their surface. This repulsion can be explained by the abundance of  $\text{H}^+$  ions competing with lead (II) ions for adsorption sites. As a result, lead (II) adsorption is diminished, leading to potential electrostatic repulsion. On the other hand, at pH 6, the negatively charged AL particles had a favorable interaction with the surface and ions, resulting in increased adsorption of lead (II) ions onto the AL surface. It has been determined that pH 6 is the optimum pH for lead (II) adsorption, with a maximum adsorption capacity of  $175 \text{ mg}\cdot\text{g}^{-1}$  (Figure 4). After pH 6, the adsorption capacity of lead (II) gradually decreased.

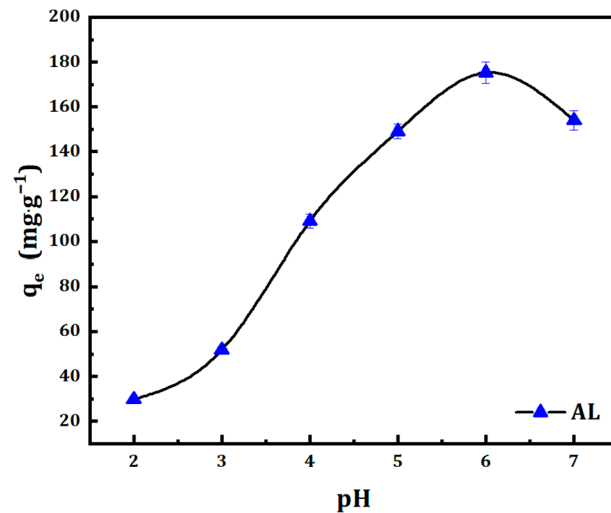


**Figure 4.** Effect of pH on the adsorption of lead (II) on activated sample.

### 3.1.2. Influence of Adsorbent Dose

To investigate the influence of the quantity of adsorbent on the adsorption of lead (II) from an aqueous solution, a series of adsorption experiments were performed. These experiments entailed varying the adsorbent amount while maintaining a pH of 6, an initial metal concentration of  $200 \text{ mg}\cdot\text{L}^{-1}$ , a shaking speed of 150 rpm, and a temperature at room temperature. As depicted in Figure 5, an augmentation in adsorbent dosage resulted in an increase in the percentage of adsorption. This effect is ascribed to the expansion of the adsorbent's surface area, enhancing the availability of binding sites for adsorption. However, beyond a specific dosage of the adsorbent, the percentage of adsorption reached a plateau. This occurs when all binding sites on the adsorbent become occupied by lead (II) ions [43]. Notably, a minimum dosage of  $0.5 \text{ g}\cdot\text{L}^{-1}$  of carbon microspheres proved adequate to achieve a maximum removal of 31.4% of lead (II).

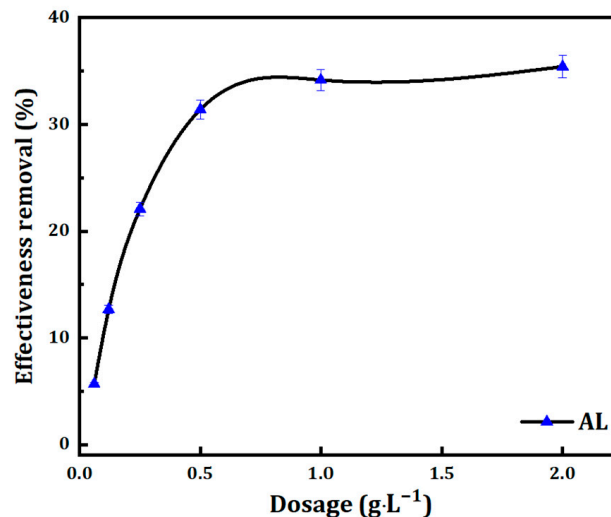


**Figure 5.** Effect of dose on adsorption of lead (II) on activated sample.

### 3.1.3. The Effect of Initial Concentration and Contact Duration

The AL sample's capability for adsorbing lead (II) solution was examined across various concentrations of the heavy metal, ranging from  $50$  to  $500 \text{ mg}\cdot\text{L}^{-1}$ . All experiments maintained a contact time of 300 min, reaching equilibrium after 60 min. Initially, the removal of lead (II) ions from the solution was rapid, gradually slowing until reaching equilibrium. Figure 6 illustrates the quantity of lead (II) adsorbed by AL at  $25 \text{ }^\circ\text{C}$ . The

prepared samples exhibited heightened adsorption capacity with increasing lead (II) concentrations. Notably, the maximum adsorption capacity reached  $136.04 \pm 5.1 \text{ mg}\cdot\text{g}^{-1}$  for AL, surpassing the adsorption capacity of UAL, which was determined to be  $51.6 \text{ mg}\cdot\text{g}^{-1}$ . It is also noteworthy that the adsorption capacity of the calcined sample (L-Cal) at  $550^\circ\text{C}$  without  $\text{H}_3\text{PO}_4$  treatment was  $94.94 \text{ mg}\cdot\text{g}^{-1}$ . These findings suggest a direct correlation: as the initial concentration of lead (II) rises, the adsorption capacity of AL also increases.

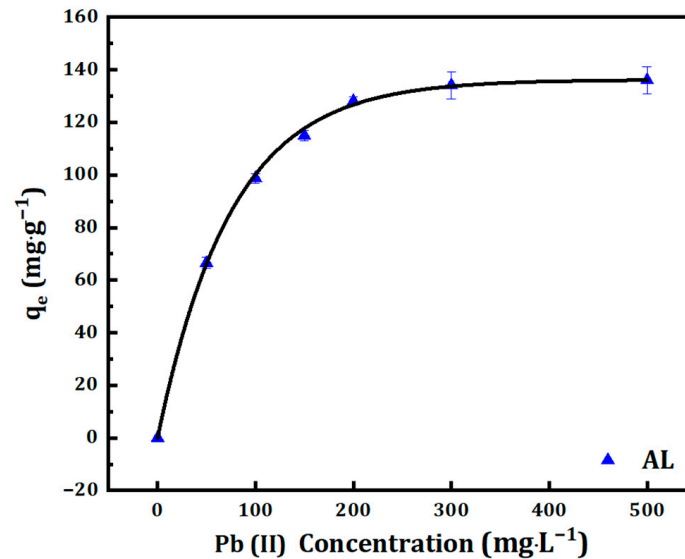


Figure 6. Adsorption capacities of activated sample.

### 3.2. Adsorption Isotherm

A graphical representation is employed to illustrate the equilibrium correlation between the sum of a substance adsorbed on a solid surface and the concentration of that substance in the surrounding fluid phase, which is referred to as the adsorption isotherm [44]. It is a valuable tool for understanding adsorption's fundamental principles and designing effective adsorption systems. The previously obtained results on the influence of initial concentration against contact time were used to analyze the adsorption isotherm models further. The linearized version of the Langmuir adsorption isotherm was utilized. All the parameters involved in each adsorption isotherm model were calculated to construct the graphical plot. Through comparing all the graphical plots, an inference can be made regarding the compatibility of the experimental data with the adsorption isotherm model, which will summarize the behavior of the adsorbate–adsorbent interaction that occurs in this batch process [45].

#### 3.2.1. Langmuir Isotherm

The model that assumes adsorption happens in a single layer on noninteracting active sites on the surface is called the Langmuir adsorption model [46], and it can be written as follows:

$$q_e = \frac{q_m K_L C_e}{1 + K_L C_e} \quad (4)$$

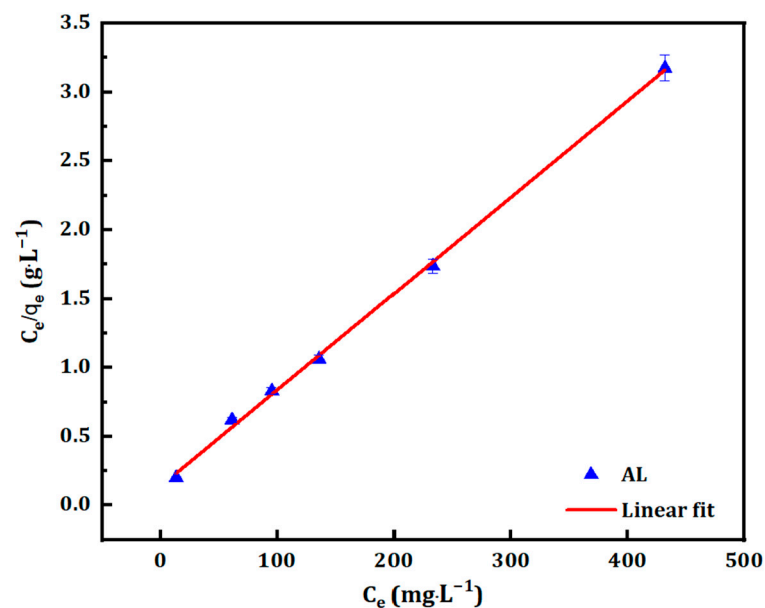
where  $q_m$  is the adsorption capacity of AL, and  $K_L$  denotes the Langmuir constant. Equation (4) can be written in a linear expression as in Equation (5), and the plot of  $(C_e/q_e)$  versus  $C_e$  is plotted, where  $q_m$  and  $K_L$  are calculated and listed in Table 3.

$$\frac{C_e}{q_e} = \frac{1}{q_m} C_e + \frac{1}{K_L q_m} \quad (5)$$

**Table 3.** Langmuir, Freundlich, Redlich–Peterson, and Temkin isotherm constants for the AL.

CM Samples	Langmuir Constants			Freundlich Constants		
	$Q_{\max}$ ( $\text{mg}\cdot\text{g}^{-1}$ )	$K_L$ ( $\text{L}\cdot\text{mg}^{-1}$ )	$R^2$	$1/n$	$K_F$ ( $\text{mg}^{1-1/n}\cdot\text{L}^{1/n}\cdot\text{g}^{-1}$ )	$R^2$
AL	142.86	0.051	0.999	0.22	39.99	0.931
	Redlich–Peterson Constants			Temkin Constants		
	$B$	$A$	$R^2$	$B$	$A$	$R^2$
AL	0.781	39.99	0.994	21.613	1.852	0.948

The Langmuir equation was strongly supported by the experimental data, as evidenced by the high linear regression value ( $R^2$ ) of 0.999 (Figure 7).

**Figure 7.** Langmuir isotherm of AL.

The Langmuir isotherm can be mathematically related to separation factor ( $R_L$ ), which is a dimensionless constant used to determine the type of adsorption process. The mathematical expression for  $R_L$  is given as follows:

$$R_L = \frac{1}{(1 + K_L C_0)} \quad (6)$$

where  $C_0$  denotes the initial concentration of lead in the solution ( $\text{mg}\cdot\text{L}^{-1}$ ). A value of  $R_L$  less than 1 indicates a favorable adsorption process, and an  $R_L$  of 1 implies a linear adsorption process. In contrast, an  $R_L$  value greater than 1 suggests an unfavorable adsorption process, and an  $R_L$  value of 0 signifies an irreversible adsorption process. In the present study, the values of  $R_L$  were between 0.0377 and 0.2817 for concentrations between 500 and 50  $\text{mg}\cdot\text{L}^{-1}$ , respectively. The obtained values indicate that the adsorption of lead (II) onto AL is a favorable process across all ranges of lead concentrations.

### 3.2.2. Freundlich Isotherm

The relationship between adsorption capacity ( $q_e$ ) and the concentration substance in the solution ( $C_e$ ) is described by the Freundlich adsorption model equation [47]. The equation is given by

$$q_e = K_F C_e^{1/n} \quad (7)$$

where  $K_F$  and  $n$  are constants, where  $K_F$  is expressed as ( $\text{mg}^{1-1/n} \cdot \text{L}^{1/n} \cdot \text{g}^{-1}$ ). The heterogeneity factor ( $1/n$ ) measures the nonlinearity of the adsorption process. A higher value of  $1/n$  indicates a more nonlinear process. When the value of  $1/n$  tends towards zero, the adsorption is said to be more heterogeneous. This means that adsorption occurs at different points on the surface and adsorption capacity is not the same at all points, and when  $1/n$  is closer to 1, the adsorption is said to be more homogeneous. This means that the adsorption takes place at all sites on the surface and that the adsorption capacity is the same at all sites [48]. The constants are figured out from the linear plot of  $\log q_e$  versus  $\log C_e$ , as in Equation (8):

$$\ln q_e = \ln K_f + \frac{1}{n} \ln C_e \quad (8)$$

The data were plotted based on the linearized Freundlich equation in Figure 8. The linear regression value,  $R^2$  for AL was 0.931.

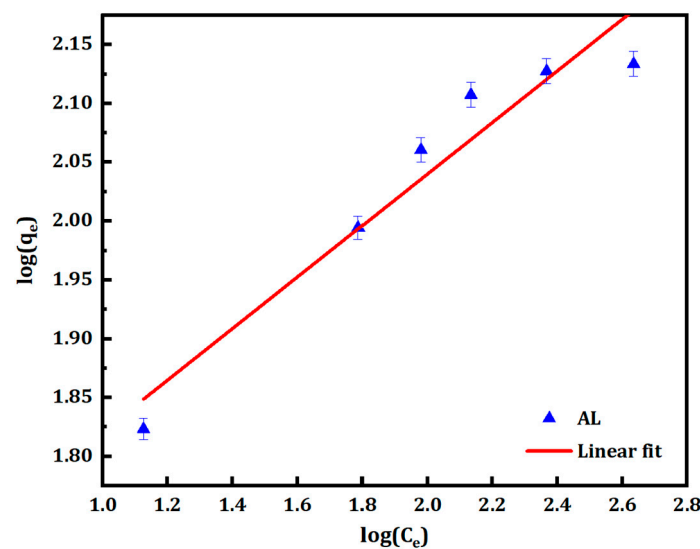


Figure 8. Freundlich isotherm of AL.

### 3.2.3. Redlich–Peterson Isotherm

The Redlich–Peterson isotherm model [49] is a hybrid model that integrates the Langmuir and Freundlich isotherm models to describe adsorption on heterogeneous surfaces. The model can be used to be applied to describe adsorption systems where the adsorbate can be adsorbed in either a single layer or multiple layers, and is a common model to study adsorption phenomena. To create a linear graphical representation of  $\ln(C_e/q_e)$  against  $\ln(C_e)$ , (Figure 9) was performed to obtain the values of  $\beta$  and  $A$ , where  $\beta$  is the slope and  $\ln A$  is the intercept. The relationship is described by Equation (9):

$$\ln\left(\frac{C_e}{q_e}\right) = \beta \ln C_e - \ln A \quad (9)$$

where  $\beta$  and  $A$  were computed and documented in Table 3. The linear regression value,  $R^2$  for AL is 0.994. The results showed that AL favorably adsorbs lead (II).

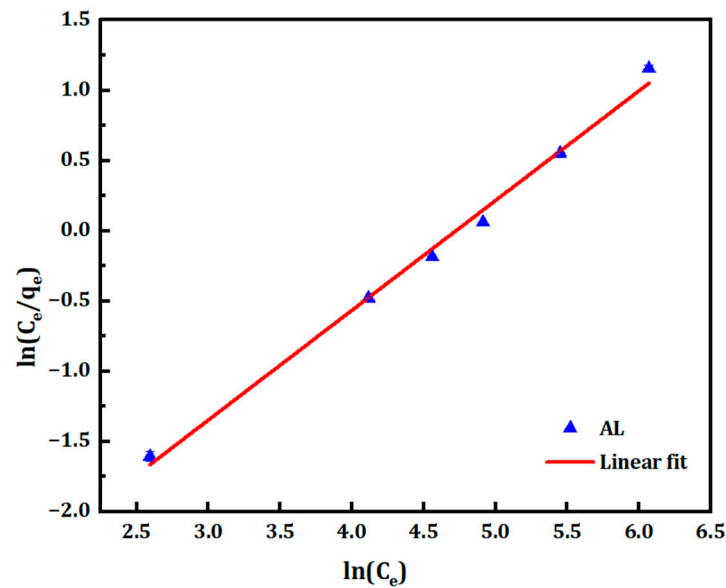


Figure 9. Redlich–Peterson isotherm of AL.

#### 3.2.4. Temkin Isotherm

The Temkin isotherm model [50] is represented by Equation (10):

$$q_e = \frac{RT}{b_T} \ln(A_T C_e) \quad (10)$$

where  $R$  is the gas constant,  $T$  is the temperature, and  $b_T$  and  $A_T$  are constants. A linearized plot can be derived to Equation (11):

$$q_e = B \ln A_T + B C_e \quad (11)$$

The isotherm assumes that the adsorption energy of each molecule is the same, but as the coverage of the adsorbent surface increases, there is a corresponding linear decrease in the value of  $q_e$ . This is because the adsorbed molecules interact with each other, reducing the free energy of each molecule [50]. This isotherm is based on the idea that all surface sites in a homogeneous material have the same affinity for the adsorbate. This means that the amount of adsorbate adsorbed onto each site will be the same, regardless of the order in which the sites are filled. The Freundlich isotherm, in contrast, does not make this assumption. It allows for the possibility that some surface sites may have a higher affinity for the adsorbate than others. This makes it more suitable for modeling adsorption on heterogeneous materials, where the surface sites may have different properties [51].

The calculated values of  $B$  and  $A_T$  are presented in Table 3, and the plot is shown in Figure 10. The linear regression value was 0.948. Compared to all  $R^2$  values listed in Table 3, the data obtained from the experiment agreed with the Langmuir isotherm and Redlich–Peterson isotherms for AL. Langmuir and Redlich–Peterson isotherm plots indicate that all the points plotted were close to the trend line, giving the highest linear regression coefficient. The fact that the heavy metal molecules in the solution did not aggregate on top of the adsorbed heavy metal molecules on the activated samples is also consistent with monolayer adsorption.

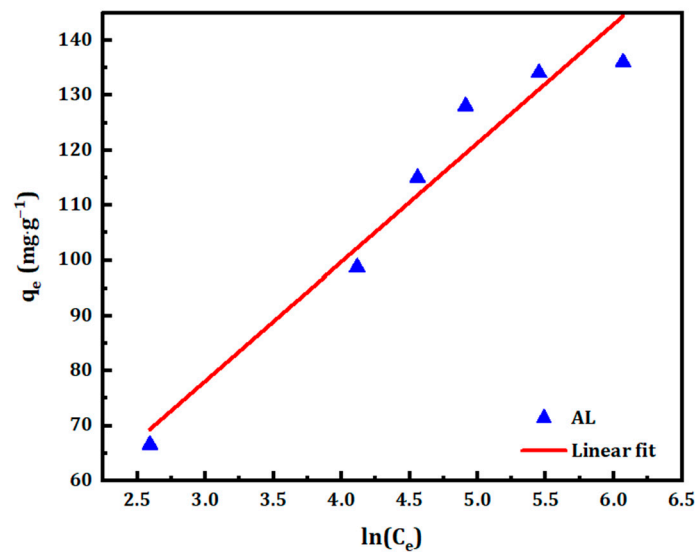


**Figure 10.** Temkin isotherm of AL.

### 3.3. Adsorption Kinetics

Adsorption kinetic analysis was used to investigate the rate of attachment of a solute onto an adsorbent material, explore the mass transfer mechanism and reaction rate, and uncover the fundamental principles that govern the adsorption process. The Lagergren pseudo-first-order kinetic model [52] and the pseudo-second-order kinetic model were employed to elucidate the dynamic of the adsorption process.

The pseudo-first-order approach operates under the core assumption that the adsorption rate is directly tied by two key factors: the availability of adsorption sites on the surface of the adsorbent and the concentration of the solute in the solution. The model can be expressed via Equation (12):

$$\ln(q_e - q_t) = \ln q_e - k_1 t \quad (12)$$

where parameter  $k_1$  represents the rate constant ( $\text{min}^{-1}$ ), further equates to the mass transfer coefficient involved in design calculations [53]. Moreover,  $t$  is the contact time. To evaluate the data, the plot of  $\ln(q_e - q_t)$  versus  $t$  was generated (Figure 11). From this, the linear regression value ( $R^2$ ) and rate parameter ( $k_1$ ) were determined and recorded in Table 4. Parameter  $k_1$  was obtained from the linear trendline slope, while adsorption capacity ( $q_e$ ) was derived from the  $y$ -intercept. For specimen AL, the linear regression was 0.9782. However, it is essential to note that the pseudo-first-order does not always accurately portray all adsorption processes, especially those involving high initial solute concentrations or adsorbents with limited adsorption abilities [54]. While this model provides one method for characterization, alternative kinetic models may prove more descriptive depending on the system and conditions.

The pseudo-second-order model can be expressed as Equation (13):

$$\frac{t}{q_t} = \frac{1}{k_2 q_e^2} + \frac{1}{q_e} t \quad (13)$$

where  $k_2$  denotes the second-order rate constant ( $\text{g} \cdot \text{min} \cdot \text{mg}^{-1}$ ). Equation (13) also includes  $q_e$  and  $q_t$ , the amounts of adsorbate adsorbed at time  $t$  (min) and at equilibrium ( $\text{mg} \cdot \text{g}^{-1}$ ), respectively. To apply this model, a  $t/q_t$  versus  $t$  plot was constructed for sample AL (Figure 12). The plot yielded values for the linear regression ( $R^2$ ) and  $k_2$  recorded in Table 4. The linear regression was 0.999. Notably, as evident from the data in Table 4, in many adsorption systems, the pseudo-second-order model often exhibits stronger mathematical correlation with experimental adsorption data compared to the pseudo-first-order model. Parameters associated with both Langmuir and Freundlich shown in Table 3 reinforce the suggestion that the chemisorption mechanism predominates in our experiment. Firstly, the

coefficient of determination for Langmuir is almost unity and higher than the coefficient of determination for Freundlich. Secondly, it is observed that  $1/n$  value is below unity, which further implies a governing chemisorption process [55,56]. Chemisorption involves the formation of chemical bonds between the lead ions and functional groups on the surface of carbon microspheres, which is expected since the activation using a relatively strong acid such as phosphoric acid would have induced such functional groups. The presence of such functional groups was also observed in our previous study [29].

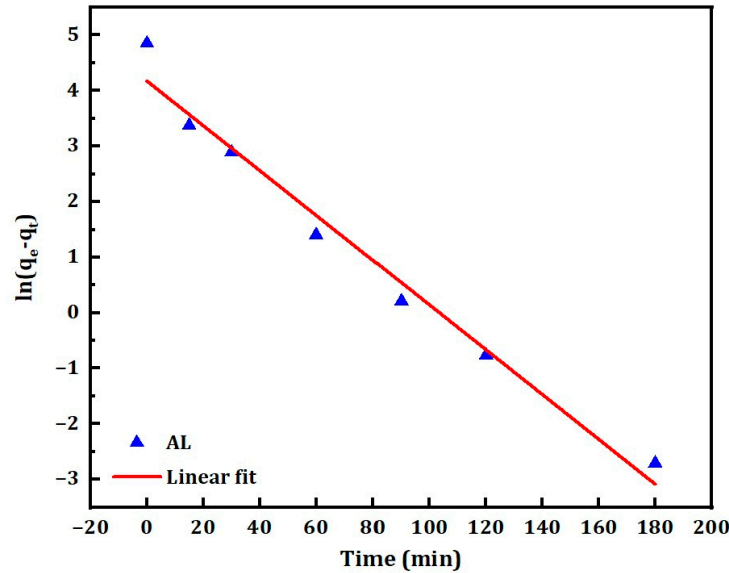


Figure 11. Pseudo-first-order kinetics for AL.

Table 4. The parameters pseudo-first-order and pseudo-second-order Kinetics for AL.

Kinetics Model	Slope	Intercept	q <sub>theo.</sub>	K	R <sup>2</sup>
Pseudo-first-order	-0.04	4.18	65.11	0.4	0.978
Pseudo-second-order	0.008	0.028	130.21	0.002	0.999

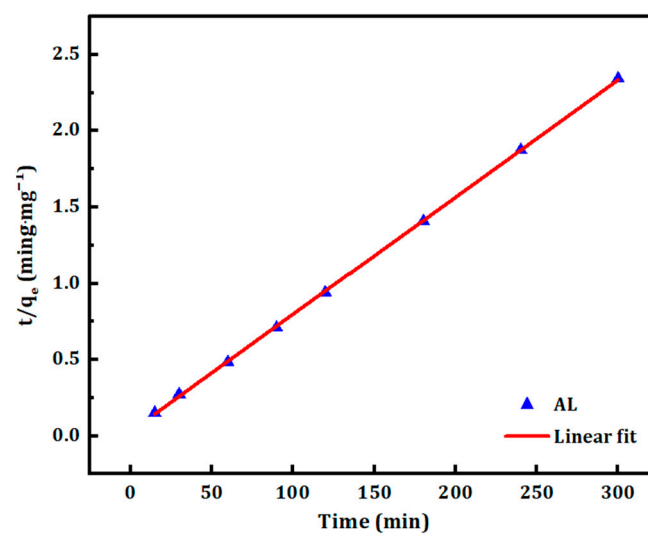


Figure 12. Pseudo-second-order kinetics for AL.

The enhanced surface area due to the treatment with phosphoric acid plays an essential role in providing ample active sites for lead ions to interact with. The formation of pores on the microspheres' surfaces contributes to increased accessibility, facilitating the adsorption

process. The pHpzc of the sample at 2.5 is vital in understanding the surface charge characteristics. At the experimental pH conditions, the carbon microsphere surface is expected to be positively charged, which may influence the electrostatic interactions with lead ions in the solution. The chemisorption mechanism involves the formation of chemical bonds between lead ions and functional groups on the surface of carbon microspheres. The activation process using phosphoric acid likely introduces functional groups, and the strength of the acid may induce the formation of reactive sites that play a crucial role in binding lead ions. In summary, the comprehensive analysis of the adsorption mechanism suggests that the unique mesoporous structure, surface charge characteristics, and probable chemisorptive interactions induced by phosphoric acid activation holistically contribute to the efficient removal of lead (II) by carbon microspheres synthesized from biomass. These insights afford a more detailed understanding of the core processes governing the adsorption behavior in our study.

A comparison of the lead (II) removal of different adsorbent-based hydrochars produced by the HTC process is summarized in Table S3.

### 3.4. Multistage Removal and Unregenerated Reuse of Adsorbent

The process of adsorption is a popular method of eliminating heavy metals from water solutions, utilizing activated materials as effective adsorbents. However, important aspects to consider in practical applications are the multistage remove and reusability of these adsorbents. The multistage adsorption was evaluated by following the evolution of the amount lead (II) along the adsorption cycles, as depicted in Figure 13A. As expected, after four successive adsorption steps, lead (II) is deeply removed and less than 4% remains. These results clearly show the high potential of AL as an adsorbent of lead (II) from aqueous solution in mild conditions.

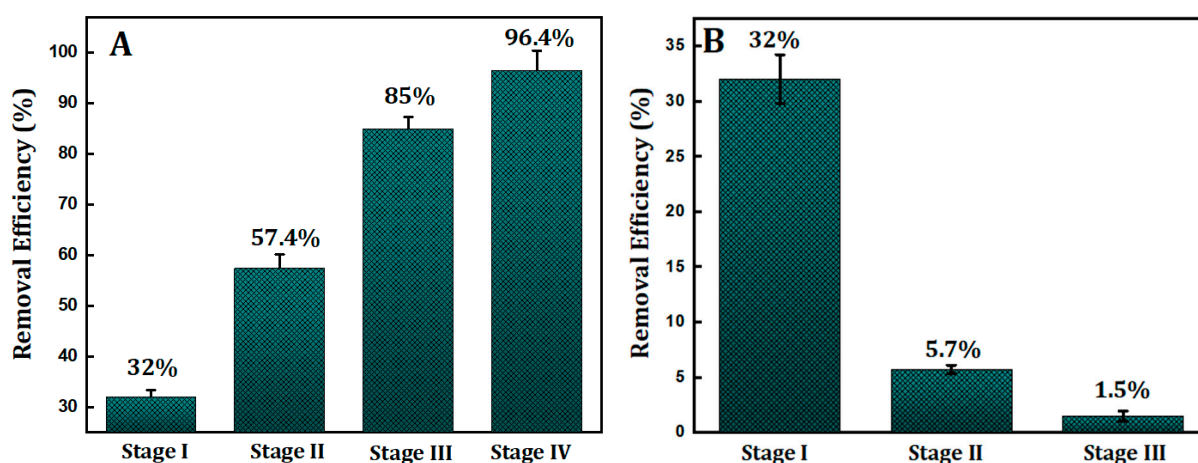


Figure 13. (A) Multistage and (B) reusability of AL.

The reusability study plays a critical role in elucidating the adsorbent transfer pathway between aqueous and solid phase. This metric provides insights into the adsorbent's ability to repeatedly capture and release lead (II) ions while maintaining its adsorption capacity. However, the evaluation of the reusability of AL was shown as a limitation of used AL to adsorb more lead (II). This underachievement is due to the saturation of its surface with lead (II), resulting in only 5.7 and 1.5% removal during the second and third reusing of AL, respectively, as presented in Figure 13B.

## 4. Environmental Implications

The use of activated carbon microspheres derived from date palm leaflets for the remediation of wastewater could be economical and beneficial. The preparation of hydrochar using microwave technology is relatively inexpensive and environmentally friendly with-

out preactivation. However, it is important to know that hydrochar has a small surface area, which impairs its adsorption capability. To overcome this obstacle, the surface area of the hydrochar can be drastically increased by various activation methods such as chemical activation using a range of chemicals, including phosphoric acid and potassium hydroxide. The activation using phosphoric acid leads to a higher level of mesopores than the activation using potassium hydroxide [57]. Nevertheless, it requires pyrolysis of the material at a high temperature of 500–600 °C. This causes additional costs for the preparation of the materials. One of the possible solutions is the introduction of functional groups on the surface of the spheres. This will be investigated in future research by functionalizing the hydrochar with other materials such as sulfonic acid or deep eutectic solvents. Intuitively, the presence of such functional groups (especially sulfonic groups) is considered beneficial for the extraction of metal ions.

## 5. Conclusions

1. Through a bespoke two-step hydrothermal carbonization–activation method, the authors created distinct and well-defined carbon microspheres from date palm biomass native to the Gulf region. Additionally, the authors described previously unreported findings on lead (II) ion adsorption onto carbon microspheres synthesized from date palm activated using phosphoric acid.
2. A minimal quantity of 0.5 g·L<sup>-1</sup> of activated carbon microspheres was sufficient to achieve a peak removal rate of 31.4% for lead (II). The findings imply that chemisorption might exert a more influence than physisorption in determining the adsorption rate for the investigated lead adsorption process.
3. This study's significance lies in its threefold impact: promoting the sustainable utilization of resources (i.e., biomass), producing valuable industrial microparticles, and offering direct use in metal-bearing wastewater purification. This data could potentially be instrumental in upscaling bench-scale adsorption systems to larger, more practical systems for water decontamination applications.

**Supplementary Materials:** The following supporting information can be downloaded at: <https://www.mdpi.com/article/10.3390/c10010026/s1>, Figure S1: Experimental determination of pH<sub>pzc</sub>. Figure S2: (a) Pore size distribution of the synthesized samples and (b) Nitrogen physisorption isotherms. Figure S3: Nonlinear fitting of adsorption isotherm models. Figure S4: Nonlinear fitting of adsorption kinetic models. Table S1: Langmuir, Freundlich, Redlich–Peterson, and Temkin isotherm constants for the AL. Table S2: Pseudo-first-order and pseudo-second-order constants for the AL. Table S3: Comparison of various adsorbent-based hydrochars prepared by the HTC process for their lead (II) removal [58–72].

**Author Contributions:** Conceptualization, M.E.-H., C.-Y.Y., S.A., A.A. and L.E.B.; methodology, M.E.-H., C.-Y.Y., L.E.B., M.M.A. and S.A.; software, M.E.-H. and S.A.; validation, M.E.-H., C.-Y.Y., S.A., M.M.A. and L.E.B.; formal analysis, M.E.-H., S.A. and C.-Y.Y.; investigation, M.E.-H., A.A. and C.-Y.Y.; resources, M.E.-H., C.-Y.Y., S.A. and L.E.B.; data curation, M.E.-H., S.A. and L.E.B.; writing—original draft preparation, M.E.-H., C.-Y.Y., S.A., M.M.A. and L.E.B.; writing—review and editing, M.E.-H., C.-Y.Y., S.A., M.M.A. and L.E.B.; visualization, M.E.-H. and C.-Y.Y.; supervision, M.E.-H. and L.E.B.; project administration, M.M.A.; funding acquisition, M.E.-H. All authors have read and agreed to the published version of the manuscript.

**Funding:** This research project was funded by the National Plan for Science, Technology, and Innovation (MAARIFAH), King Abdulaziz City for Science and Technology, Kingdom of Saudi Arabia, award no. (ENV3120-02-12).

**Data Availability Statement:** The data presented in this study are available on request from the corresponding author.

**Conflicts of Interest:** The authors declare no conflict of interest.

## References

1. Karkra, R.; Kumar, P.; Bansod, B.K.; Bagchi, S.; Sharma, P.; Krishna, C.R. Classification of heavy metal ions present in multi-frequency multi-electrode potable water data using evolutionary algorithm. *Appl. Water Sci.* **2017**, *7*, 3679–3689. [[CrossRef](#)]
2. Elbasiouny, H.; Darwesh, M.; Elbeltagy, H.; Abo-Alhamd, F.G.; Amer, A.A.; Elsegaïy, M.A.; Khattab, I.A.; Elsharawy, E.A.; Ebehiry, F.; El-Ramady, H.; et al. Ecofriendly remediation technologies for wastewater contaminated with heavy metals with special focus on using water hyacinth and black tea wastes: A review. *Environ. Monit. Assess.* **2021**, *193*, 449. [[CrossRef](#)]
3. Kamarudzaman, A.N.; Adan, S.N.A.C.; Hassan, Z.; Wahab, M.A.; Makhtar, S.M.Z.; Seman, N.A.A.; Jalil, M.F.A.; Handayani, D.; Syafiuddin, A. Biosorption of copper (II) and Iron (II) using spent mushroom compost as biosorbent. *Biointerface Res. Appl. Chem.* **2022**, *12*, 7775–7786. [[CrossRef](#)]
4. Salami, B.A.; Oyehan, T.A.; Gambo, Y.; Badmus, S.O.; Tanimu, G.; Adamu, S.; Lateef, S.A.; Saleh, T.A. Technological trends in nanosilica synthesis and utilization in advanced treatment of water and wastewater. *Environ. Sci. Pollut. Res.* **2022**, *29*, 42560–42600. [[CrossRef](#)]
5. Eccles, H. Treatment of metal-contaminated wastes: Why select a biological process? *Trends Biotechnol.* **1999**, *17*, 462–465. [[CrossRef](#)] [[PubMed](#)]
6. Crini, G.; Lichtfouse, E. Advantages and disadvantages of techniques used for wastewater treatment. *Environ. Chem. Lett.* **2019**, *17*, 145–155. [[CrossRef](#)]
7. Da'ana, D.A.; Zouari, N.; Ashfaq, M.Y.; Abu-Dieyeh, M.; Khraisheh, M.; Hijji, Y.M.; Al-Ghouthi, M.A. Removal of toxic elements and microbial contaminants from groundwater using low-cost treatment options. *Curr. Pollut. Rep.* **2021**, *7*, 300–324. [[CrossRef](#)]
8. Dutta, S.; Bhaumik, A.; Wu, K.C.W. Hierarchically porous carbon derived from polymers and biomass: Effect of interconnected pores on energy applications. *Energy Environ. Sci.* **2014**, *7*, 3574–3592. [[CrossRef](#)]
9. Wei, X.; Jiang, X.P.; Liu, X.; Zhou, W.M.; Garba, Z.N.; Lawan, L.; Wang, L.W.; Yuan, Z.H. Adsorption of organic dyes from wastewater by metal-doped porous carbon materials. *J. Clean. Prod.* **2021**, *284*, 124773. [[CrossRef](#)]
10. Hayoun, B.; Escudero-Curiel, S.; Bourouina, M.; Bourouina-Bacha, S.; Sanromán, M.A.; Pazos, M. Preparation and characterization of high performance hydrochar for efficient adsorption of drugs mixture. *J. Mol. Liq.* **2022**, *353*, 118797. [[CrossRef](#)]
11. Diaz, E.; Manzano, F.J.; Villamil, J.; Rodriguez, J.J.; Mohedano, A.F. Low-cost activated grape seed-derived hydrochar through hydrothermal carbonization and chemical activation for sulfamethoxazole adsorption. *Appl. Sci.* **2019**, *9*, 5127. [[CrossRef](#)]
12. Diaz, E.; Sanchis, I.; Coronella, C.J.; Mohedano, A.F. Activated carbons from hydrothermal carbonization and chemical activation of olive stones: Application in sulfamethoxazole adsorption. *Resources* **2022**, *11*, 43. [[CrossRef](#)]
13. Adebisi, G.A.; Chowdhury, Z.Z.; Abd Hamid, S.B.; Ali, E. Hydrothermally treated banana empty fruit bunch fiber activated carbon for Pb (II) and Zn (II) removal. *BioResources* **2016**, *11*, 9686–9709. [[CrossRef](#)]
14. Shi, J.; Cui, H.; Xu, J.; Yan, N. Carbon spheres synthesized from  $\text{KHCO}_3$  activation of glucose derived hydrochar with excellent  $\text{CO}_2$  capture capabilities at both low and high pressures. *Sep. Purif. Technol.* **2022**, *294*, 121193. [[CrossRef](#)]
15. Congsomjit, D.; Areeprasert, C. Hydrochar-derived activated carbon from sugar cane bagasse employing hydrothermal carbonization and steam activation for syrup decolorization. *Biomass Convers. Biorefinery* **2021**, *11*, 2569–2584. [[CrossRef](#)]
16. Koprivica, M.; Simić, M.; Petrović, J.; Ercegović, M.; Dimitrijević, J. Evaluation of adsorption efficiency on Pb (II) ions removal using alkali-modified hydrochar from paulownia leaves. *Processes* **2023**, *11*, 1327. [[CrossRef](#)]
17. Zhang, Y.; Wan, Y.; Zheng, Y.; Yang, Y.; Huang, J.; Chen, H.; Quan, G.; Gao, B. Potassium permanganate modification of hydrochar enhances sorption of Pb (II), Cu (II), and Cd (II). *Bioresour. Technol.* **2023**, *386*, 129482. [[CrossRef](#)]
18. Acharya, S. Lead between the lines. *Nat. Chem.* **2013**, *5*, 894. [[CrossRef](#)]
19. Chowdhury, I.R.; Chowdhury, S.; Mazumder, M.A.J.; Al-Ahmed, A. Removal of lead ions ( $\text{Pb}^{2+}$ ) from water and wastewater: A review on the low-cost adsorbents. *Appl. Water Sci.* **2022**, *12*, 185. [[CrossRef](#)]
20. Kumar, A.; Kumar, A.; Cabral-Pinto, M.M.S.; Chaturvedi, A.K.; Shabnam, A.A.; Subrahmanyam, G.; Mondal, R.; Gupta, D.K.; Malyan, S.K.; Kumar, S.S.; et al. Lead toxicity: Health hazards, influence on food chain, and sustainable remediation approaches. *Int. J. Environ. Res. Public Health* **2020**, *17*, 2179. [[CrossRef](#)]
21. Rasmey, A.H.; Aboeidah, A.A.; Youssef, A.K. Application of Langmuir and Freundlich isotherm models on biosorption of  $\text{Pb}^{2+}$  by freeze-dried biomass of *Pseudomonas aeruginosa*. *Egypt. J. Microbiol.* **2018**, *53*, 37–48. [[CrossRef](#)]
22. Nzediegwu, C.; Naeth, M.A.; Chang, S.X. Lead (II) adsorption on microwave-pyrolyzed biochars and hydrochars depends on feedstock type and production temperature. *J. Hazard. Mater.* **2021**, *412*, 125255. [[CrossRef](#)]
23. Rasam, S.; Moraveji, M.K.; Soria-Verdugo, A.; Salimi, A. Synthesis, characterization and adsorbability of *Crocus sativus* petals hydrothermal carbonized hydrochar and activated hydrochar. *Chem. Eng. Process. Process Intensif.* **2021**, *159*, 108236. [[CrossRef](#)]
24. Petrović, J.T.; Stojanović, M.D.; Milojković, J.V.; Petrović, M.S.; Šoštarić, T.D.; Laušević, M.D.; Mihajlović, M.L. Alkali modified hydrochar of grape pomace as a perspective adsorbent of  $\text{Pb}^{2+}$  from aqueous solution. *J. Environ. Manag.* **2016**, *182*, 292–300. [[CrossRef](#)] [[PubMed](#)]
25. Zhou, N.; Chen, H.; Feng, Q.; Yao, D.; Chen, H.; Wang, H.; Zhou, Z.; Li, H.; Tian, Y.; Lu, X. Effect of phosphoric acid on the surface properties and Pb (II) adsorption mechanisms of hydrochars prepared from fresh banana peels. *J. Clean. Prod.* **2017**, *165*, 221–230. [[CrossRef](#)]
26. Ge, Q.; Tian, Q.; Wang, S.; Zhang, J.; Hou, R. Highly efficient removal of lead/cadmium by phosphoric acid-modified hydrochar prepared from fresh banana peels: Adsorption mechanisms and environmental application. *Langmuir* **2022**, *38*, 15394–15403. [[CrossRef](#)]

27. Al-Awadi, A.S.; El-Harbawi, M.; Algarawi, A.; Alalawi, A.; Alrashed, M.M.; Yin, C.Y. Synthesis of carbon microspheres via hydrothermal carbonization of Sabal palms (*Sabal palmetto*) biomass for adsorption of methylene blue. *Biomass Convers. Biorefin.* **2022**, *2022*, 16943–16953. [[CrossRef](#)]
28. El-Harbawi, M.; Alhawtali, S.; Al-Awadi, A.S.; El Blidi, L.; Alrashed, M.M.; Alzobidi, A.; Yin, C.Y. Synthesis of carbon microspheres from inedible crystallized date palm molasses: Influence of temperature and reaction time. *Materials* **2023**, *16*, 1672. [[CrossRef](#)]
29. Alhawtali, S.; El-Harbawi, M.; Al-Awadi, A.S.; El Blidi, L.; Alrashed, M.M.; Yin, C.Y. Enhanced adsorption of methylene blue using phosphoric acid-activated hydrothermal carbon microspheres synthesized from a variety of palm-based biowastes. *Coatings* **2023**, *13*, 1287. [[CrossRef](#)]
30. Romero-Anaya, A.J.; Lillo-Ro'denas, M.A.; Salinas-Martínez de Lecea, C.; Linares-Solano, A. Hydrothermal and conventional H<sub>3</sub>PO<sub>4</sub> activation of two natural bio-fibers. *Carbon* **2012**, *50*, 3158–3169. [[CrossRef](#)]
31. Romero-Anaya, A.J.; Ouzzine, M.; Lillo-Rodenas, M.A.; Linares-Solano, A. Spherical carbons: Synthesis, characterization and activation processes. *Carbon* **2014**, *68*, 296–307. [[CrossRef](#)]
32. Rivera-Utrilla, J.; Bautista-Toledo, I.; Ferro-García, M.A.; Moreno-Castilla, C. Activated carbon surface modifications by adsorption of bacteria and their effect on aqueous lead adsorption. *J. Chem. Technol. Biotechnol.* **2001**, *76*, 1209–1215. [[CrossRef](#)]
33. Órfão, J.J.M.; Silva, A.I.M.; Pereira, J.C.V.; Barata, S.A.; Fonseca, I.M.; Faria, P.C.C.; Pereira, M.F.R. Adsorption of a reactive dye on chemically modified activated carbons—Influence of pH. *J. Colloid Interface Sci.* **2006**, *296*, 480–489. [[CrossRef](#)]
34. Baccile, N.; Weber, J.; Falco, C.; Titirici, M.M. Characterization of hydrothermal carbonization materials. In *Sustainable Carbon Materials from Hydrothermal Processes*; Titirici, M.-M., Ed.; John Wiley & Sons: Hoboken, NJ, USA, 2013; pp. 151–211. [[CrossRef](#)]
35. Nasser, R.A.; Salem, M.Z.; Hiziroglu, S.; Al-Mefarrej, H.A.; Mohareb, A.S.; Alam, M.; Aref, I.M. Chemical analysis of different parts of date palm (*Phoenix dactylifera* L.) using ultimate, proximate and thermo-gravimetric techniques for energy production. *Energies* **2016**, *9*, 374. [[CrossRef](#)]
36. Dong, X.; Guo, S.; Wang, H.; Wang, Z.; Gao, X. Physicochemical characteristics and FTIR-derived structural parameters of hydrochar produced by hydrothermal carbonisation of pea pod (*Pisum sativum* Linn.) waste. *Biomass Convers. Biorefinery* **2019**, *9*, 531–540. [[CrossRef](#)]
37. Reza, M.T.; Wirth, B.; Lüder, U.; Werner, M. Behavior of selected hydrolyzed and dehydrated products during hydrothermal carbonization of biomass. *Bioresource Technol.* **2014**, *169*, 352–361. [[CrossRef](#)] [[PubMed](#)]
38. Ameen, M.; Zamri, N.M.; May, S.T.; Aziz, M.T.; Aqsha, A.; Sabzoi, N.; Sher, F. Effect of acid catalysts on hydrothermal carbonization of Malaysian oil palm residues (leaves, fronds, and shells) for hydrochar production. *Biomass Convers. Biorefinery* **2022**, *12*, 103–114. [[CrossRef](#)]
39. Sisuthog, W.; Attanatho, L.; Chaiya, C. Conversion of empty fruit bunches (EFBs) by hydrothermal carbonization towards hydrochar production. *Energy Rep.* **2022**, *8*, 242–248. [[CrossRef](#)]
40. Garrido, J.A.; Härtl, A.; Kuch, S.; Stutzmann, M.; Williams, O.A.; Jackmann, R.B. pH sensors based on hydrogenated diamond surfaces. *Appl. Phys. Lett.* **2005**, *86*, 1866632. [[CrossRef](#)]
41. Issabayeva, G.; Aroua, M.K.; Sulaiman, N.M.N. Removal of lead from aqueous solutions on palm shell activated carbon. *Bioresour. Technol.* **2006**, *97*, 2350–2355. [[CrossRef](#)]
42. Mullet, M.; Fievet, P.; Szymczyk, A.; Foissy, A.; Reggiani, J.C.; Pagetti, J. A simple and accurate determination of the point of zero charge of ceramic membranes. *Desalination* **1999**, *121*, 41–48. [[CrossRef](#)]
43. Saifuddin, M.N.; Kumaran, P. Removal of heavy metal from industrial wastewater using chitosan coated oil palm shell charcoal. *Electron. J. Biotechnol.* **2005**, *8*, 44–53.
44. Tee, W.T.; Hiew, B.Y.Z.; Thangalazhy-Gopakumar, S.; Gan, S.; Lee, L.Y. Biochar as a remediation solution for pharmaceutical-contaminated wastewater. In *BioChar: Applications for Bioremediation of Contaminated Systems*; Walter de Gruyter: Berlin, Germany, 2022; p. 373.
45. Lafi, R.; ben Fradj, A.; Hafiane, A.; Hameed, B.H. Coffee waste as potential adsorbent for the removal of basic dyes from aqueous solution. *Korean J. Chem. Eng.* **2014**, *31*, 2198–2206. [[CrossRef](#)]
46. Langmuir, I. The constitution and fundamental properties of solids and liquids. Part I. Solids. *J. Am. Chem. Soc.* **1916**, *38*, 2221–2295. [[CrossRef](#)]
47. Freundlich, H. Über die Adsorption in Lösungen [Adsorption in solution]. *Z. Für Phys. Chem. J. Phys. Chem.* **1907**, *57*, 385–470. [[CrossRef](#)]
48. Fytianos, K.; Voudrias, E.; Kokkalis, E. Sorption-desorption behaviour of 2, 4-dichlorophenol by marine sediments. *Chemosphere* **2000**, *40*, 3–6. [[CrossRef](#)]
49. Redlich, O.J.D.L.; Peterson, D.L. A useful adsorption isotherm. *J. Phys. Chem.* **1959**, *63*, 1024. [[CrossRef](#)]
50. Temkin, M.I. Adsorption equilibrium and kinetics of processes on nonhomogeneous surfaces and at interaction between adsorbed molecules. *Zhurnal Fiz. Khimii J. Phys. Chem.* **1941**, *15*, 296–332.
51. Demir-Cakan, R.; Baccile, N.; Antonietti, M.; Titirici, M.-M. Carboxylate-rich carbonaceous materials *via* one-step hydrothermal carbonization of glucose in the presence of acrylic acid. *Chem. Mater.* **2009**, *21*, 484–490. [[CrossRef](#)]
52. Lagergren, S. Zur Theorie der Sogenannten Adsorption gelöster Stoffe [To the theory of the so-called adsorption of dissolved materials]. *K. Sven. Vetenskapsakademiens Handl.* **1898**, *24*, 1–39. [[CrossRef](#)]
53. Gupta, V.K. and Suhas Application of Low-Cost Adsorbents for Dye Removal—A Review. *J. Environ. Manag.* **2009**, *90*, 2313–2342. [[CrossRef](#)]

54. Ho, Y.S.; McKay, F.G. Kinetic models for the sorption of dye from aqueous solution by wood. *Process Saf. Environ. Prot.* **1998**, *76*, 183–191. [[CrossRef](#)]
55. Zhang, X.; Zhao, J.; Cheng, L.; Lu, C.; Wang, Y.; He, X.; Zhang, W. Acrylic acid grafted and acrylic acid/sodium humate grafted bamboo cellulose nanofibers for Cu<sup>2+</sup> adsorption. *RSC Adv.* **2014**, *4*, 55195–55201. [[CrossRef](#)]
56. Hernández-Francisco, E.; Bonilla-Cruz, J.; Márquez-Lamas, U.; Suárez-Jacobo, Á.; Longoria-Rodríguez, F.; Rivera-Haro, J.; Russell, P.; Ali, Z.; Yin, C.Y.; Lara-Ceniceros, T.E. Entangled cellulose nanofibrils/nanosheets derived from native mexican agave for lead (II) ion removal. *Cellulose* **2020**, *27*, 8785–8798. [[CrossRef](#)]
57. Niinipuu, M.; Latham, K.G.; Jansson, S. The influence of inorganic components and carbon-oxygen surface functionalities in activated hydrothermally carbonized waste materials for water treatment. *Environ. Sci. Pollut. Res.* **2020**, *27*, 38072–38083. [[CrossRef](#)]
58. Ding, Z.; Zhang, L.; Mo, H.; Chen, Y.; Hu, X. Microwave-assisted catalytic hydrothermal carbonization of *Laminaria japonica* for hydrochars catalyzed and activated by potassium compounds. *Bioresour. Technol.* **2021**, *341*, 125835. [[CrossRef](#)]
59. Xia, Y.; Yang, T.; Zhu, N.; Li, D.; Chen, Z.; Lang, Q.; Liu, Z.; Jiao, W. Enhanced adsorption of Pb (II) onto modified hydrochar: Modeling and mechanism analysis. *Bioresour. Technol.* **2019**, *288*, 121593. [[CrossRef](#)]
60. Ahmad, S.; Zhu, X.; Luo, J.; Shen, M.; Zhou, S.; Zhang, S. Conversion of phosphorus and nitrogen in lincomycin residue during microwave-assisted hydrothermal liquefaction and its application for Pb<sup>2+</sup> removal. *Sci. Total Environ.* **2019**, *687*, 1381–1388. [[CrossRef](#)]
61. Ahmad, S.; Zhu, X.; Wang, Q.; Wei, X.; Zhang, S. Microwave-assisted hydrothermal treatment of soybean residue and chitosan: Characterization of hydrochars and role of N and P transformation for Pb (II) removal. *J. Anal. Appl. Pyrolysis* **2021**, *160*, 105330. [[CrossRef](#)]
62. Jia, Y.; Zhang, Y.; Fu, J.; Yuan, L.; Li, Z.; Liu, C.; Zhao, D.; Wang, X. A novel magnetic biochar/MgFe-layered double hydroxides composite removing Pb<sup>2+</sup> from aqueous solution: Isotherms, kinetics and thermodynamics. *Colloids Surf. A Physicochem. Eng. Asp.* **2019**, *567*, 278–287. [[CrossRef](#)]
63. Guo, S.; Gao, Y.; Wang, Y.; Liu, Z.; Wei, X.; Peng, P.; Xiao, B.; Yang, Y. Urea/ZnCl<sub>2</sub> in situ hydrothermal carbonization of *Camellia sinensis* waste to prepare N-doped biochar for heavy metal removal. *Environ. Sci. Pollut. Res.* **2019**, *26*, 30365–30373. [[CrossRef](#)]
64. Guo, S.; Wang, Y.; Wei, X.; Gao, Y.; Xiao, B.; Yang, Y. Structural analysis and heavy metal adsorption of N-doped biochar from hydrothermal carbonization of *Camellia sinensis* waste. *Environ. Sci. Pollut. Res.* **2020**, *27*, 18866–18874. [[CrossRef](#)]
65. Chen, Y.; Xu, F.; Li, H.; Li, Y.; Liu, Y.; Chen, Y.; Li, M.; Li, L.; Jiang, H.; Chen, L. Simple hydrothermal synthesis of magnetic MnFe<sub>2</sub>O<sub>4</sub>-sludge biochar composites for removal of aqueous Pb<sup>2+</sup>. *J. Anal. Appl. Pyrolysis* **2021**, *156*, 105173. [[CrossRef](#)]
66. Luo, X.; Huang, Z.; Lin, J.; Li, X.; Qiu, J.; Liu, J.; Mao, X. Hydrothermal carbonization of sewage sludge and in-situ preparation of hydrochar/MgAl-layered double hydroxides composites for adsorption of Pb (II). *J. Clean. Prod.* **2020**, *258*, 120991. [[CrossRef](#)]
67. Liu, D.; Tang, Y.; Li, J.; Hao, Z.; Zhu, J.; Wei, J.; Liu, C.; Dong, L.; Jia, B.; Chen, G. Eupatorium adenophorum derived adsorbent by hydrothermal-assisted HNO<sub>3</sub> modification and application to Pb<sup>2+</sup> adsorption. *J. Environ. Chem. Eng.* **2021**, *9*, 105972. [[CrossRef](#)]
68. Wang, B.; Yu, J.; Liao, H.; Zhu, W.; Ding, P.; Zhou, J. Adsorption of lead (II) from aqueous solution with high efficiency by hydrothermal biochar derived from honey. *Int. J. Environ. Res. Public Health* **2020**, *17*, 3441. [[CrossRef](#)]
69. Yang, W.; Wang, Z.; Song, S.; Han, J.; Chen, H.; Wang, X.; Sun, R.; Cheng, J. Adsorption of copper (II) and lead (II) from seawater using hydrothermal biochar derived from *Enteromorpha*. *Mar. Pollut. Bull.* **2019**, *149*, 110586. [[CrossRef](#)]
70. Ramesh, S.; Sundararaju, P.; Banu, K.S.P.; Karthikeyan, S.; Doraiswamy, U.; Soundarapandian, K. Hydrothermal carbonization of arecanut husk biomass: Fuel properties and sorption of metals. *Environ. Sci. Pollut. Res.* **2019**, *26*, 3751–3761. [[CrossRef](#)]
71. Chowdhury, Z.Z.; Krishnan, B.; Sagadevan, S.; Rafique, R.F.; Hamizi, N.A.B.; Abdul Wahab, Y.; Khan, A.A.; Johan, R.B.; Al-Douri, Y.; Kazi, S.N.; et al. Effect of temperature on the physical, electro-chemical and adsorption properties of carbon micro-spheres using hydrothermal carbonization process. *Nanomaterials* **2018**, *8*, 597. [[CrossRef](#)]
72. Hammud, H.H.; Karnati, R.K.; Al Shafee, M.; Fawaz, Y.; Holail, H. Activated hydrochar from palm leaves as efficient lead adsorbent. *Chem. Eng. Commun.* **2021**, *208*, 197–209. [[CrossRef](#)]

**Disclaimer/Publisher’s Note:** The statements, opinions and data contained in all publications are solely those of the individual author(s) and contributor(s) and not of MDPI and/or the editor(s). MDPI and/or the editor(s) disclaim responsibility for any injury to people or property resulting from any ideas, methods, instructions or products referred to in the content.